Journal of Rainwater Catchment Systems Vol.13/No.1/pp.11-16

Journal of Rainwater Catchment Systems

Numerical Experiments of the Effects of Obstructions Shape Variation on the Flow in Nature-like Fishways

Subas Chhatkuli[1] and Masayuki Fujihara[2]

Abstract: This paper presents the variation in key flow properties due to the standard deviation of obstruction shape variation in nature-like fishways, using a Godunov type numerical method of two dimensional shallow water equations. Elliptic obstructions having different aspect ratios are embedded in the model fishway. The variation of shape is evaluated from the standard deviation of diameter length. The change in flow parameters because of the increment in the standard deviation of shape variation was compared from four different test cases. The increment in the standard deviation showed a distinct effect on the flow parameters. Increase in standard deviation showed the decrease in the area occupied by higher velocities, as well as increase in variation of flow velocities. Likewise, the increase in standard deviation raised the average water depth in the fishways.

Keywords: *Shallow water equation; Elliptical obstructions; Roe's approximate Riemann Solver; Finite volume method; Godunov type method*

1 Introduction

Modeling of flow past obstructions of various shapes has long been an interest to scientist and engineers. In the field of hydraulic engineering, obstructions of various shapes have been constantly used for flow control. Recently, the application of obstructions for controlling flow to create a favorable flow conditions in fishways is getting popular. This kind of fishways, which is termed as nature-like fishways or rocky ramp fishways, essentially consists of a sloping channel embedded with a set of natural or artificial obstructions. The key factors that engineering designer should consider while designing such kinds of fishways are shorter fish pathways, deeper water depths to enable big fish to take fishways and larger lower velocity region for fish to take rest. Though these kinds of fishways mimic the flow of a natural streams and are considered favorable for large species of fish as well as invertebrates, the widespread construction of such kinds of fishways has been constrained by the lack of concrete design guidelines.

Acharya *et al.* (2000) and Kells *et al.* (2000) presented a discussion of the nature-like fishways with specific focus on several aspects of their design. Miyazono *et al.* (2005) investigated the characteristics of this type of fishways through hydraulic model experiments and fish release test. In the previous researches, cylindrical obstructions with perfect circular, rectangular or triangular shapes have been considered. However, elliptical or oval obstructions would approximate the natural shape of boulders better than the perfect circular shape. Previous researches have shown that flow past elliptical obstructions behaves differently than flow past circular obstructions. Hence the research on flow properties around the elliptical obstructions is important for the better and more accurate understanding of the flow characteristics in the nature-like fishways.

Faruquee *et al.* (2007) did study on the effects of axis ratio on laminar fluid flow around an elliptical cylinder. They noted that the wake size increased as the axis ratio (AR) increased from 0.4. Likewise, the drag coefficient was found to increase with the increase of AR. The drag coefficient was maximum for AR = 1 (circular cylinder). Johnson *et al.* (2004) examined the nominally two-dimensional wake behind elliptical bodies at low Reynolds numbers using numerical simulation as the body geometry is changed from a flat plate normal to the free stream flow to that of a circular cylinder. Onset of asymmetry was studied for cylinder and elliptical cylinders by Nair and Sengupta (1996). They noted that while the circular cylinder flow remained symmetric for a long time, the flow field around the elliptical cylinders at zero incidence became asymmetric earlier. Furthermore, the asymmetry developed at a faster rate for the thicker ellipse.

The most of the earlier studies of flow past elliptical cylinders focused mostly on the flow past isolated elliptical obstacle. In this study gross effect of multiple elliptical obstacles with different aspect ratios are analyzed. The change in flow parameters because of the increment in the standard deviation (SD) of shape variation has been numerically compared from four different test cases using a Godunov type numerical method of two dimensional Shallow Water Equations (SWEs).

2 Governing Equations and Numerical Model

SWEs describe flow in shallow water bodies where the vertical acceleration can be neglected and then the pressure becomes hydrostatic. Hence the continuity of mass and momentum equations can be integrated over the depth and solved numerically to give the depth averaged velocity fields.

Depth averaged conservation of mass and momentum equations used are as follows (Rogers *et al.*, 2001).

[1]Ph.D student, The United Graduate School of Agricultural Sciences, Ehime University, 3-5-7 Tarumi, Matsuyama-shi, Ehime, 790-8566 Japan

[2]Professor, Faculty of Agriculture, Ehime University, 3-5-7 Tarumi, Matsuyama-shi, Ehime, 790-8566 Japan

$$\frac{\partial \zeta}{\partial t}+\frac{\partial (uh)}{\partial x}+\frac{\partial (vh)}{\partial y}=0 \tag{1}$$

$$\frac{\partial (uh)}{\partial t}+\frac{\partial (u^2h+\frac{1}{2}g(\zeta^2+2\zeta h_s))}{\partial x}+\frac{\partial (uvh)}{\partial y} -\nu_t\left(\frac{\partial (hu_x)}{\partial x}+\frac{\partial (hu_y)}{\partial y}\right)=-\frac{\tau_{bx}}{\rho}-g\zeta S_{ox} \tag{2}$$

$$\frac{\partial (vh)}{\partial t}+\frac{\partial (uvh)}{\partial x}+\frac{\partial (v^2h+\frac{1}{2}g(\zeta^2+2\zeta h_s))}{\partial y} -\nu_t\left(\frac{\partial (hv_x)}{\partial x}+\frac{\partial (hv_y)}{\partial y}\right)=-\frac{\tau_{by}}{\rho}-g\zeta S_{oy} \tag{3}$$

where ζ is the free surface elevation above the still water level h_s, $h(=\zeta+h_s)$ the total water depth, u and v the depth-averaged velocities in the x and y directions respectively, u_x, u_y and v_x, v_y the derivatives of the depth averaged velocity components in the x and y directions respectively, g the acceleration due to gravity, ρ water density, τ_{bx} and τ_{by} the bed friction stresses in x and y directions respectively, ν_t the kinematic eddy viscosity coefficient and S_{ox} and S_{oy} the bed slopes in the x and y directions respectively.

The kinematic eddy viscosity is expressed by Smagorinsky model as follows,

$$\nu_t=(c\Delta)^2\left[2\left(\frac{\partial u}{\partial x}\right)^2+\left(\frac{\partial u}{\partial y}+\frac{\partial v}{\partial x}\right)^2+2\left(\frac{\partial v}{\partial y}\right)^2\right]^{1/2} \tag{4}$$

in which

$$\Delta=(\Delta x\cdot\Delta y)^{1/2}$$

where c is the Smagorinsky constant and $\Delta x, \Delta y$ are the computational cell lengths in the x and y directions respectively.

The bed shear stress terms are evaluated by using a turbulent shear type model:

$$\tau_{bx}=\rho C_f u\sqrt{u^2+v^2} \tag{5}$$

$$\tau_{by}=\rho C_f v\sqrt{u^2+v^2} \tag{6}$$

where C_f is an empirical coefficient based on bed roughness given by:

$$C_f=\frac{m^2 g}{R^{1/3}} \tag{7}$$

where m is the Manning's coefficient and R the hydraulic radius.

Integrating Eqs. (1) - (3) over a control volume (Ω) and by applying Gauss' theorem (Fujihara and Borthwick, 2000; Rogers *et al.* 2001), we get

$$\frac{\partial}{\partial t}\int_\Omega \mathbf{Q}d\Omega+\oint_\Psi \mathbf{F}\cdot\mathbf{n}d\Psi=\int_\Omega \mathbf{H}d\Omega \tag{8}$$

where

$$\mathbf{Q}=\begin{bmatrix}\zeta\\ uh\\ vh\end{bmatrix},$$

$$\mathbf{F}=\begin{bmatrix} uh & vh\\ u^2h+\frac{1}{2}g(\zeta^2+2\zeta h_s)-\nu_t h\frac{\partial u}{\partial x} & uvh-\nu_t h\frac{\partial u}{\partial y}\\ uvh-\nu_t h\frac{\partial v}{\partial x} & v^2h+\frac{1}{2}g(\zeta^2+2\zeta h_s)-\nu_t h\frac{\partial v}{\partial y}\end{bmatrix},$$

$$\mathbf{H}=\begin{bmatrix}0\\ -\frac{\tau_{bx}}{\rho}-g\zeta S_{ox}\\ -\frac{\tau_{by}}{\rho}-g\zeta S_{oy}\end{bmatrix},$$

Ψ the boundary of Ω and $\mathbf{n}$ the unit normal vector through Ψ.

The flux in Eq. (8) can be written in terms of inviscid and viscid form

$$\mathbf{F}\cdot\mathbf{n}=\mathbf{f}^I-\nu_t\mathbf{f}^V \tag{9}$$

in which

$$\mathbf{f}^I=\begin{bmatrix} uhn_x+vhn_y\\ \left(u^2h+g\left[\zeta^2+2\zeta h_s\right]/2\right)n_x+uvhn_y\\ uvhn_x+\left(v^2h+g\left[\zeta^2+2\zeta h_s\right]/2\right)n_y\end{bmatrix}$$

and

$$\mathbf{f}^V=\begin{bmatrix}0\\ (h\partial u/\partial x)n_x+(h\partial u/\partial y)n_y\\ (h\partial v/\partial x)n_x+(h\partial v/\partial y)n_y\end{bmatrix}$$

where n_x and n_y are Cartesian components of $\mathbf{n}$.

The SWEs are discretised on quadtree girds with conserved variables (ζ, uh and vh) stored at the cell center of each computational cell. The inviscid fluxes are evaluated by adopting Roe's approximate Riemann solver at each cell edge (Fujihara *et al.* 2003). The inter cell inviscid flux $\mathbf{f}^I_{i,j}$ is evaluated as

$$\mathbf{f}^I_{i,j}=1/2\left[\mathbf{f}^I\left(\mathbf{Q}^+_{i,j}\right)+\mathbf{f}^I\left(\mathbf{Q}^-_{i,j}\right)-|\mathbf{A}|\left(\mathbf{Q}^+_{i,j}-\mathbf{Q}^-_{i,j}\right)\right] \tag{10}$$

in which

$$|\mathbf{A}|=\mathbf{R}|\mathbf{\Lambda}|\mathbf{L} \tag{11}$$

where $\mathbf{Q}^{+}_{i,j}$ and $\mathbf{Q}^{-}_{i,j}$ are reconstructed right and left Riemann states respectively at the cell interface located between adjacent cells i and j and $\mathbf{A}$ the flux Jacobian using $\mathbf{R}$ and $\mathbf{L}$, the right and left eigenvector matrices of $\mathbf{A}$ respectively. The symbol $|\mathbf{\Lambda}|$ in Eq. (11) denotes a diagonal matrix of the absolute values of the eigen values of $\mathbf{A}$.

The viscous fluxes are evaluated by using central difference approximation and fourth order Runge-Kutta scheme is used for the temporal integration.

The minmod limiter is selected as a slope limiter in a computational cell where the values of variables are linearly distributed so that the numerical scheme employed becomes a second-order approximation (Hirsch, 1990).

Riemann invariants, specified according to the local Froude number, have been used to implement open boundary condition (Fujihara and Borthwick, 2000).

3 Model Validation

The numerical model is validated against the physical model experiments conducted by Miyazono *et al.* (2005). They reported the flow pattern in a sloping channel with semi-circular boulders embedded with a straight line (Case A) and a zigzag line (Case B). The physical model experiment was conducted on a 3.6 m long and 1 m wide ramp with slope 1:10. Horizontal channel of 1 m length was attached at the beginning and at the end of the slope. Five semi-circular boulders of diameter 0.23 m were set at 0.4 m interval longitudinally for Case A and Case B. In the physical model experiment at the upstream boundary, discharge (Q) was set 0.053 m^3/s and water depth at the upstream boundary (H) was set 0.125 m for Case A. For Case B, Q and H were 0.064 m^3/s and 0.125 m respectively. The same boundary conditions, boulder configuration, size and slope of the ramp were set for the computational purpose. Manning's roughness coefficient was 0.011 $m^{-1/3}s$ and Smagorinsky constant was 0.2.

In the physical model experiment conducted for Case A, the velocity contour of 1 m/s transversely extended from the wall of the channel to the edge of the first boulder. After that, the contour extended longitudinally along the boulders edges from the first boulder to the last boulder.

Considering the physical model results for Case B, velocity contour of 0.6 m/s started from the edge of the first boulder and ends nearly at the centre of the second boulder. The velocity contour of 0.6 m/s started from the edge of second boulder and ended at the edge of the third boulder. This alternate pattern was seen for the remaining boulders respectively. Considering the 1 m/s velocity contour, along the left potion of the boulders, it extended transversely from the wall of the channel to the first boulder. After then, the contour continued longitudinally along the boulders touching the alternate boulders.

The very similar velocity contour was obtained by the numerical modeling which is shown in Figure 1. This shows that the model can simulate flow around multiple obstructions realistically and with a sound accuracy.

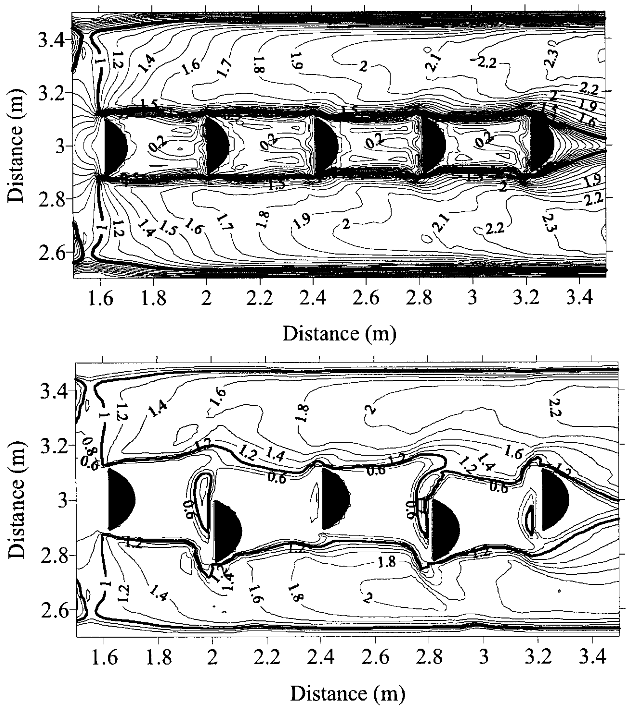

Figure 1: Velocity contour for Case A (Top) and Case B (Bottom)

4 Experimental Cases

The experimental cases consist of four test cases. In all the four test cases, in a 4 m long and 2 m wide sloping ramp obstructions of varying shapes were embedded in a regular pattern. Since bottom gradient 1/20 appears to be the most common in nature-like fishways (Kells *et al.*, 2000), the bottom gradient of the ramp was set to be 1/20 in all the cases. Upstream and downstream of the sloping ramp was connected to the straight channel of 2 m length and 2 m width. At the upstream, water depth 0.2 m was set as a boundary condition. At the downstream end, water depth 0.2 m was set as boundary condition when the flow was sub-critical. For the super-critical outflow conditions inner state of Riemann values were assigned as a boundary condition.

For the first experimental case, Case I, the diameter (=A) of obstructions in longitudinal direction (X- direction) and the diameter (=B) of them in transverse direction (Y- direction) both were set 0.2 m. Hence the aspect ratio (A: B) was 1 (Circular). In the other experimental Cases II, III and IV, 'A' was kept constant and 'B' was varied to get the elliptical shapes of obstructions. In Case II, 'B' was varied randomly against the mean diameter of 0.2 m with the standard deviation (SD) of 2.5 cm. In Case III and Case IV, the standard deviations were 5 cm and 10 cm, respectively.

36 elliptic obstructions were embedded on the ramp and the longitudinal and transverse intervals of them were 0.5 m and 0.4 m, respectively.

Figure 2 shows the distribution of diameters of obstructions in Y-direction (B) for the three test cases.

Manning's roughness coefficient was 0.011 $m^{-1/3}s$ and Smagorinsky constant was 0.2.

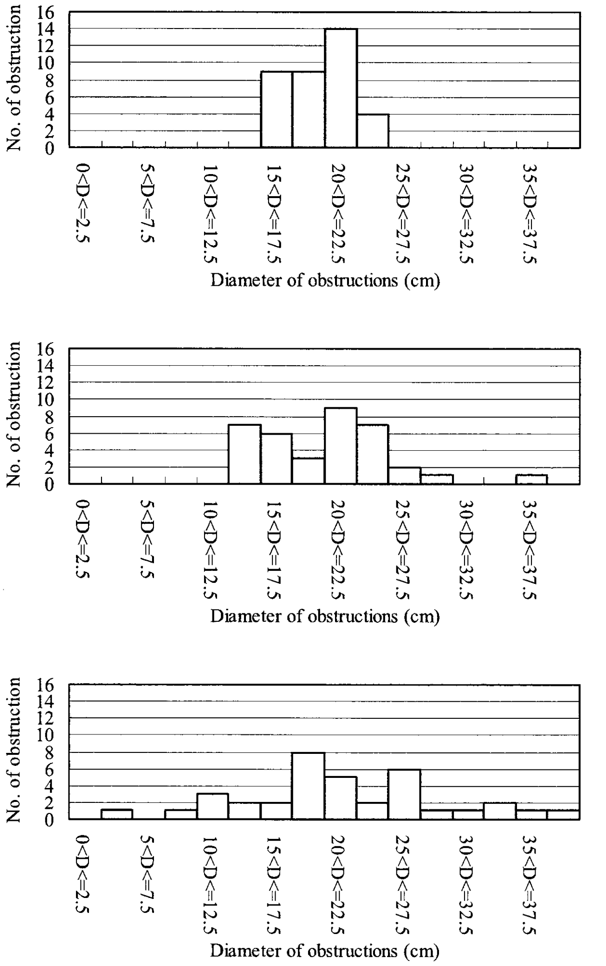

Figure 2: Distribution of diameters of obstructions in Y direction for Case II, Case III and Case IV (top, middle and bottom respectively)

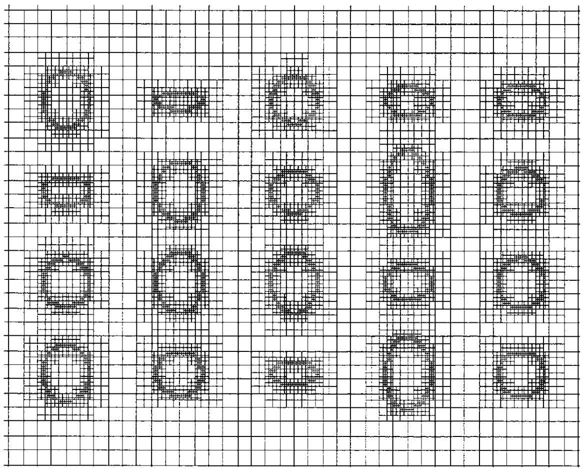

Figure 3: Quadtree grid for CASE IV.

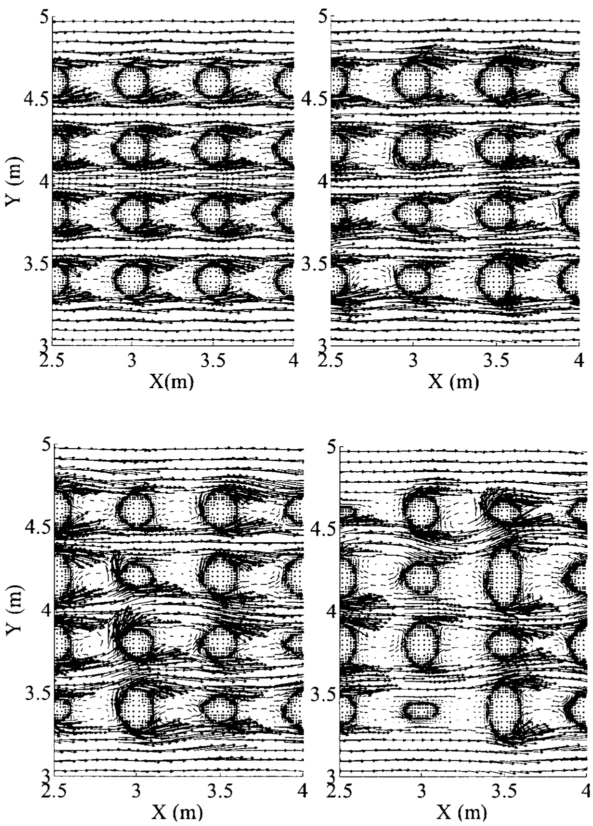

Figure 4: Time averaged velocity vectors for Case I(Top left), Case II (Top right), Case III (Bottom left) and Case IV (Bottom right)

5 Results and Discussion

Figure 3 shows the quadtree grid generated for CASE IV. Maximum size of the grid was 6.25 cm x 6.25 cm and minimum size was 0.78 cm x 0.78 cm.

Simulation time of all experiments was 110 seconds. The numerical results of unsteady flow for last 20 seconds were used for obtaining averaged values. Since the region from 2.5 m to 4 m, in X- direction, was independent of back water effect, the area was considered for the analysis purpose.

5.1 Velocity

Figure 4 shows the time averaged velocity vectors for the four cases. Figure 5 is the velocity contours for the same. From the figures, we can see, roughly, the velocity in the wake region is less than 0.2 m/s and that in the primary flow region (between obstructions placed set side - by - side) is over 1 m/s.

The velocity distributions in the fishway for the four cases are depicted in Figure 6. From the figures, the distinct effect of the SD of shape variation can be noted on the velocity distribution pattern especially in the lower and higher velocity distribution trend. The lower velocity region ($V <=$ 0.2 m/s) was 21%, 21%, 18% and 24% for Case I, II, III and IV, respectively. The corresponding net diameter of obstructions in Y- direction directly intercepting the flow was 3.20 m, 3.16 m, 3.24 m and 3.26 m for the Cases I, II, III and IV, respectively. In Case III, though the net diameter

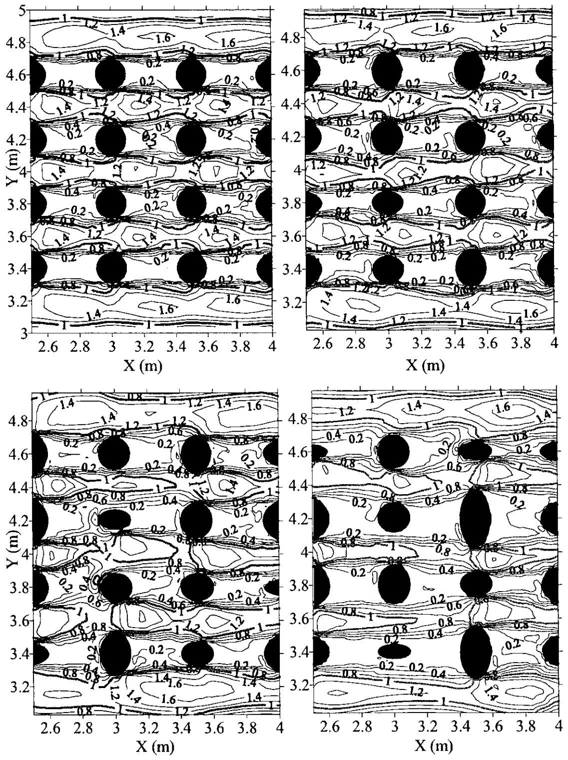

Figure 5: Time averaged velocity contours for Case I (Top left), Case II (Top right), Case III (Bottom left) and Case IV (Bottom right)

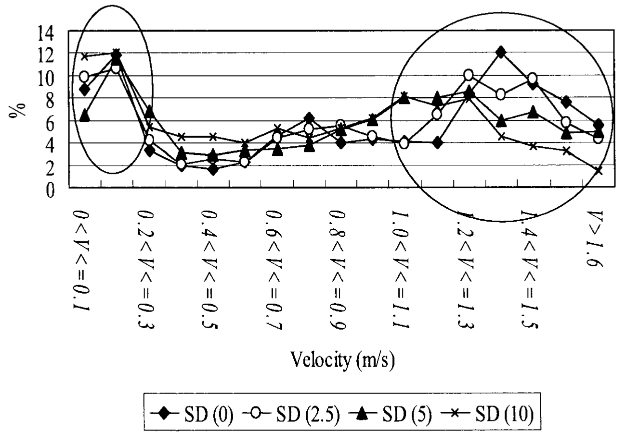

Figure 6: Velocity Distributions for Case I (SD = 0cm), Case II (SD = 2.5 cm), Case III (SD = 5 cm) and Case IV (SD= 10cm)

in Y- direction was greater than in Case I and II, the corresponding lower velocity region was lower. Though it seems natural that increasing the total length of obstruction diameters in Y- direction will create a larger lower velocity region, this was not observed from the experiments. This might be due to the layout of the obstructions with different axis ratios.

Considering the velocity more than or equal to 1.0 m/s (V>= 1.0 m/s), the study shows that increasing the SD of shape variation of obstructions will decrease the area covered by higher velocities. For Case I, the area with V>= 1.0 m/s was 51%. For Case II, III and IV, they were 48%, 47%

Table 1: Mean velocity (V_m) and SD of velocity (SD_v) against SD of shape variation of obstructions (SD) in all experimental cases.

CASE	SD (cm)	V_m (m/s)	SD_v (m/s)
I	0	0.91	0.61
II	2.5	0.88	0.58
III	5	0.86	0.56
IV	10	0.73	0.51

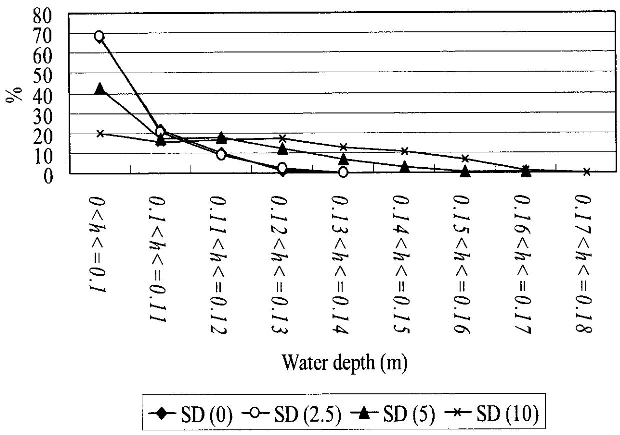

Figure 7: Water depth distributions for Case I (SD = 0 cm), Case II (SD = 2.5 cm), Case III (SD = 5 cm) and Case IV (SD= 10 cm)

and 36%, respectively.

Looking at the trend of the higher velocity distribution, Figure 6, it is clear that the increase in SD of shape variation flattens the distribution curve of higher velocity. This trend suggests that when the SD of shape variation increases the two distinct flow patterns i.e. jet flow through the gap and nearly stagnant flow behind the obstructions will start to be less prominent and the overall moderate flow will occur.

Table 1 shows the change in mean velocity and SD of velocity by increasing the SD of shape variation of obstructions. The results show that increasing the SD of shape variation will reduce the mean velocity of the flow. Moreover, the reduction in SD of velocity with the increase in SD of shape variation suggests that when the SD of shape variation is higher more areas in the channel will have flow near to the mean velocity.

5.2 Water depth

Figure 7 shows the water depth distribution pattern for the four test cases. In Case I and II there was no such significant difference in water depth distribution patterns. For both of the cases areas occupied by lower water depth (h <= 0.1 m) were about 68%. While increasing the SD of shape variation of obstruction, areas occupied by lower water depth (h <= 0.1 m) in Cases III and IV reduced to about 42% and 20% respectively. The result showed that the area of lowest water depth decreases with increase in SD of shape variation of obstructions. Likewise, the in-

Table 2: Mean water depth (h_m) and SD of water depth (SD_h) against SD of shape variation of obstructions (SD) in all experimental cases.

CASE	SD (cm)	h_m (m)	SD_h (m)
I	0	0.093	0.017
II	2.5	0.093	0.003
III	5	0.104	0.024
IV	10	0.120	0.024

crease in SD of shape variation of obstructions increased the maximum water depth. The maximum water depths in Case I and II were about 0.14 m. In Case III and IV it was increased to about 0.18 m.

Table 2 shows the change in mean water depth and SD of water depth with change in SD of shape variation in the channel. The results showed that with the increase in SD of shape variation of obstructions, mean water depth also increases.

6 Conclusions

The primary conclusions that can be drawn from the study are as follows:

(1) Increasing SD of shape variation of obstructions will decrease the area covered by higher velocities.
(2) Increment in SD of shape variation will reduce the mean velocity of flow.
(3) Increment in SD of shape variation will decrease the SD of velocity.
(4) Area of lowest water depth will decrease with an increment in SD of shape variation.
(5) Maximum water depth in a channel will elevate with the increase in SD of shape variation.
(6) Mean water depth in a channel will rise with the increment in SD of shape variation.

Increasing the SD of obstruction shape variation creates more variation in velocity and water depth distributions. Hence, when various fish species are targeted in constructing nature-like fishways, shape variation of obstructions should be considered.

Acknowledgements

This work has been supported by the Japan Society for the Promotion of Sciences through Grant-in-Aid for Scientific Research No. 18580246. The numerical experiments was conducted by FUJITSU PRIMEPOWER HPC2500 in Institute for Information Management and Communication, Kyoto Univeristy.

References

[1] Acharya, M., Kells, J. E., and Katopodis, C. (2000): Some hydraulic design aspects of nature-like fishways, *Proc. Conference on water resources engineering and water resources planning & management,* ASCE, Minneapolis, July, USA, pp.1-10.

[2] Faruquee, Z., Ting, D.S-K., Fartaj, A., Barron, R.M., and Carriveau, R. (2007): The effects of axis ratio on laminar fluid flow around an elliptical cylinder, *Int. J. Heat Fluid Flow*, doi:10.1016/j.ijheatfluidflow.2006.11.004.

[3] Fujihara, M., and Borthwick, A. G. L. (2000): Godunov-type solution of curvilinear shallow-water equations, *J. of Hydr. Engrg,* 126(11), pp.827-836.

[4] Fujihara, M., Fukushima, T., and Tachibana, K. (2003): Numerical investigation of flow in vertical single-and double-slot fishways, *Trans. JSIDRE*, 223, pp.79-88.

[5] Johnson, S.A., Thompson, M.C., and Hourigan, K. (2004): Predicted low frequency structures in the wake of elliptical cylinders, *European Journal of Mechanics B/Fluids*, 23, pp.229-239

[6] Kells, J. E., Acharya, M., and Katopodis, C. (2000): Design of nature-like fishways for small dam projects, *Proc. 3rd Annual Conf,* Canadian Dam Association, Regina, Canada, pp. 85-91.

[7] Miyazono, M., Takauji, T., and Tomatsu, O. (2005): Hydraulic characteristics and natorial action of fish around boulders, *J. Jap. Soc. Erosion Control Eng*, 57(5), pp.15-24 (in Japanese with English abstract).

[8] Nair, M.T., and Sengupta, T. K. (1996): Onset of asymmetry: Flow past circular and elliptical cylinders, *International Journal for Numerical methods in Fluids*, 23, pp.1327-1345.

[9] Rogers, B., Fujihara, M., and Borthwick. A. G. L. (2001): Adaptive Q-tree Godunov-type scheme for shallow water equations, *Int. J. Numer. Meth. Fluids*, 35, pp.247-280.

Discussion open until June 30, 2008